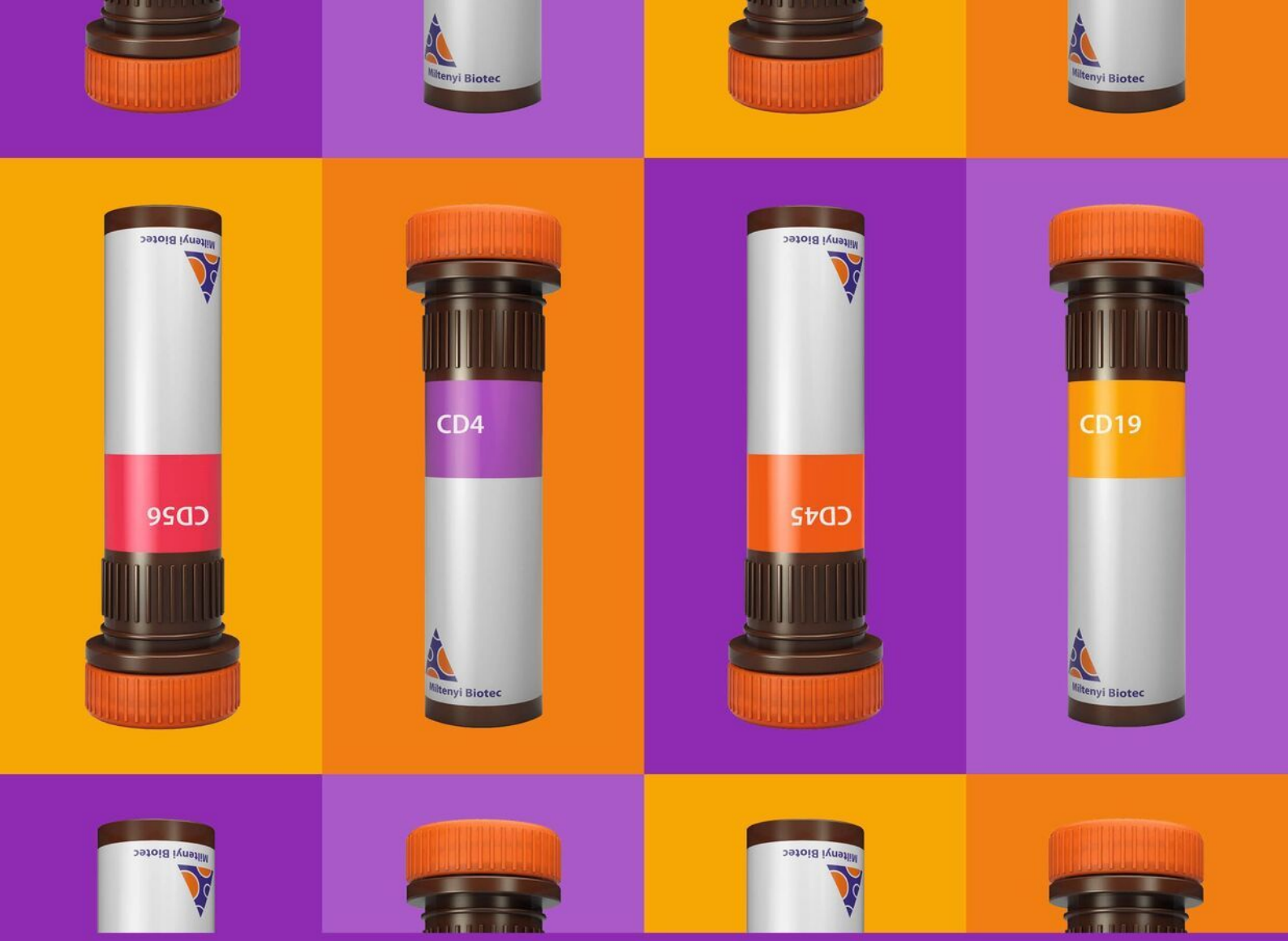

What if rethinking your antibodies ...

... could revolutionize your flow cytometry?

Recombinant antibodies are crucial to enable reproducible results. In order to confidentially switch from monoclonal to recombinant antibodies Miltenyi Biotec conducts an extensive in-house validation program. It includes testing sensitivity, and specificity through knock-out validation, and comparison to other hybridoma clones on the market. Rethink your antibodies to secure your research over many years.

▸ **miltenyibiotec.com/antibody-validation**

Miltenyi Biotec B.V. & Co. KG | Phone +49 2204 8306-0 | Fax +49 2204 85197
macsde@miltenyi.com | **www.miltenyibiotec.com**

Miltenyi Biotec provides products and services worldwide. Visit **www.miltenyibiotec.com/local** to find your nearest Miltenyi Biotec contact.

Miltenyi Biotec

Received: 24 February 2023 | Revised: 3 August 2023 | Accepted: 18 August 2023

DOI: 10.1002/cyto.a.24787

ORIGINAL ARTICLE

MIFlowCyt

ISAC INTERNATIONAL SOCIETY FOR ADVANCEMENT OF CYTOMETRY

CYTOMETRY Journal of Quantitative Cell Science PART A

HLA DQ protein changes the cell surface distribution pattern of HLA proteins as monitored by Förster resonance energy transfer and high-resolution electron microscopy

József Kormos[1] | Adrienn J. Veres[1] | László Imre[1] | László Mátyus[1] | Szilvia Benkő[2] | János Szöllősi[1,3] | Attila Jenei[1,4]

[1]Department of Biophysics and Cell Biology, Faculty of Dentistry, University of Debrecen, Debrecen, Hungary

[2]Department of Physiology, Faculty of Medicine, University of Debrecen, Debrecen, Hungary

[3]ELKH-DE Cell Biology and Signaling Research Group (Eötvös Loránd Research Network-University of Debrecen), Faculty of Medicine, University of Debrecen, Debrecen, Hungary

[4]Department of Basic Medical Sciences, Faculty of Dentistry, University of Debrecen, Debrecen, Hungary

Correspondence
Attila Jenei, Department of Biophysics and Cell Biology, Faculty of Dentistry, University of Debrecen, Egyetem tér 1, H-4032 Debrecen, Hungary.
Email: jenei@edu.unideb.hu

Abstract

Peptide presentation by MHC class I and MHC class II molecules plays important roles in the regulation of the immune response. One factor in these displays is the density of antigen, which must exceed a critical threshold for the effective activation of T cells. Nonrandom distribution of MHC class I and class II has already been detected at the nanometer level and at higher hierarchical levels. It is not clear how the absence and reappearance of some protein molecules can influence the nonrandom distribution. Therefore, we performed experiments on HLA II-deficient bare lymphocyte syndrome (BLS1) cells: we created a stable transfected cell line, tDQ6-BLS-1, and were able to detect the effect of the appearance of HLA-DQ6 molecules on the homo and hetero-association of different cell surface molecules by comparing Förster resonance energy transfer (FRET) efficiency on transfected cells to that on nontransfected BLS-1 and JY human B-cell lines. Our FRET results show a decrease in homoassociation FRET between HLA I chains in HLA-DQ6-transfected tDQ6-BLS-1 cells compared with the parent BLS-1 cell line and an increase in heteroassociation FRET between HLA I and HLA II (compared with JY cells), suggesting a similar pattern of antigen presentation by the HLA-DQ6 allele. Transmission electron microscopy (TEM) revealed that both HLA class I and class II molecules formed clusters at higher hierarchical levels on the tDQ6-BLS-1 cells, and the de novo synthesized HLA DQ molecules did not intersperse with HLA class I islands. These observations could be important in understanding the fine tuning of the immune response.

KEYWORDS
BLS-1, FRET, HLA-DQ6, immunogold labeling, MHC, TEM

1 | INTRODUCTION

MHC molecules are cell surface molecules that present processed peptides to T cells to initiate tolerance or adaptive immune responses.

József Kormos and Adrienn J. Veres contributed equally to this article.

They are grouped into two major classes, MHC class I and class II, that differ in many aspects, including expression, structure, and the type of antigen presented [1]. Class I MHC molecules are expressed on nucleated cells and present a variety of peptides to $CD8^+$ T cells, thereby activating these cells and engendering effector responses to targets displaying corresponding MHC I/peptide complexes [2, 3]. MHC II proteins are expressed constitutively on professional antigen-presenting cells (such as macrophages); however, their expression may also be induced in cell types that are closely related to innate immune and inflammatory responses, such as endothelial and epithelial cells. MHC II peptides are presented to CD4+ T cells, and they have become of great interest in various immunotherapies and approaches, such as developing vaccines against tumors [4] or viral infections. [5]. One important factor in antigen presentation is the antigen density, which must exceed some critical threshold for the effective activation of T cells, as low density may be anergic rather than stimulatory. The requisite density may be achieved by the mutual recruitment of MHC/peptide and TcR in immunologic synapses to increase the local antigen density and signal strength [6]. Conversely, dispersing endogenous clusters of MHC II molecules by disrupting lipid rafts lowers the effectiveness of the antigen [7]. Clustering has mainly been defined for MHC II molecules on many distance scales [8, 9]. In contrast, MHC I synapses have not shown the same clustering formation of MHC I as for MHC II [10]. MHC I clusters are too small to be resolved by light microscopy; however, larger clusters can be detected by advanced imaging techniques and analysis [11, 12]. Clustered MHC molecules may be more effective in immune synapses because the cluster presents a sustained signal by virtue of the number of TcR that can be engaged serially in the small area of a cluster [13, 14] or because clustered receptors interact to propagate conformational changes that enhance signaling [15, 16].

We expect large patches of MHC I molecules to have a high probability of containing multiple copies of the same peptide/MHC I. Hence, they will increase the avidity for T cells more strongly than more dispersed MHC I molecules. This higher avidity can enhance responses to dominant CTL epitopes. It also has the potential to broaden a CTL response by recruiting T cells with low affinity for other epitopes presented in the patch. Patching of MHC class I molecules may also increase overall cell avidity by enhancing CD8 interactions with MHC I clusters.

The cell surface distribution of membrane proteins can be studied by Förster resonance energy transfer (FRET) at the single-cell level, and a nonrandom distribution pattern of MHC class I molecules was observed over a distance range of 2–10 nm [17–22]. A second, nonrandom, and larger-scale topological organization of the MHC class I antigens was detected by indirect immunogold labeling and imaging by transmission electron microscopy (TEM) [23]. MHC class II molecules showed homoclustering and partial coclustering with MHC class I molecules by FRET. In addition, TEM studies revealed clustering of MHC II molecules at a higher hierarchical level (>20 nm) and showed that a fraction of MHC class II molecules heteroclustered with MHC class I molecules [24]. This larger-scale topological organization of the MHC class I and II antigens may perform significant functions in cell-to-cell contacts and signal transduction.

In the human population, there are no diseases accompanied by the total lack of HLA genes, which suggests that proteins encoded by these genes have such an important role that their complete lack might be fatal for the development of the fetus. The disease characterized by the total or partial lack of HLA II genes is called bare lymphocyte syndrome (BLS), which is a primary immune deficiency [25]. A typical feature of the disease is that neither HLA II proteins nor their appropriate mRNA can be detected in any of the patients' cells. For this reason, it can be presumed that genetic failure develops at the level of gene transcription and affects regulatory mechanisms that are responsible for both constitutive and induced synthesis. The genetic analysis of B-lymphocytes isolated from patients with BLS supplied essential information regarding the DNA-level regulation of HLA II genes. From these inspections, we know that in several BLS patients, the reduced HLA II expression is caused not by the malfunction of HLA genes but rather by the failure of the RFX nuclear factor or by mutation of the gene encoding the CIITA-regulating protein. BLS-1 and BLS-2 cell lines were isolated from patients with BLS [26] who had no HLA class II expression on the cell surface. Transfection of the BLS-1 cell line with the *DQA1*0102* and *DQB1*0602* alleles was able to restore HLA class II expression, in this case, the expression of HLA DQ6 molecules.

The experiments proposed here aim to test the hypothesis that cell surface expression of HLA class I and class II molecules can interfere at two levels: (1) at the nanometer scale (monitored by FRET) and (2) at a higher hierarchical level (detected by TEM). To this end, three cell lines were analyzed: the BLS-1 cell line, which has no class II expression but does have endogenous class I expression; the tDQ6-BLS-1 cell line, which expresses transfected HLA DQ (class II) and endogenous HLA class I molecules; and the JY cell line, which endogenously possesses both class I and class II molecules at sufficient levels. We investigated homo and heteroassociations of HLA class I, HLA class II, and intercellular adhesion molecule 1 (ICAM-1) cell surface molecules. We found that the association pattern of these molecules on the tDQ6-BLS-1 cells was different from that on the parent BLS-1 cells but was comparable with that of the JY cells. TEM analysis revealed that both HLA class I and class II molecules formed clusters at higher hierarchical levels on the tDQ6-BLS-1 cells similar to those observed on JY cells; however, in contrast to JY cells, the de novo synthesized HLA DQ molecules did not intersperse with HLA class I clusters.

2 | MATERIALS AND METHODS

All materials were purchased from Sigma–Aldrich (St. Louis, MO, USA) unless indicated otherwise.

2.1 | Cell culture

The human B lymphoma cell lines JY (ATCC, Manassas, VA, USA) and BLS-1 (generously provided by Prof. Mark Exley, Harvard Medical School, Boston, USA) were grown to subconfluency with three

intermittent splits in a week in RPMI 1640 medium containing 10% fetal calf serum (FCS), 2 mM L-glutamine, and 50 μg/mL gentamycin in an incubator maintained at 37°C with a 5% CO_2 atmosphere. The HLA-DQ6-transfected BLS-1 cell line (tDQ6-BLS) and the HLA-DQB1-transfected BLS-1 cell line (tDQB1-BLS-1) were cultured under similar conditions but in the presence of 200 μg/mL G418 (Geneticin) as a continual drug.

2.2 | Antibodies

Monoclonal antibodies reactive against HLA-A, B, C (IgG2aκ as W6/32), β_2 microglobulin (IgG1κ as L368), ICAM-1 (IgG1 as P2A4), and HLA-DQ and DR (IgG2a as anti HLA-DQ) were prepared from culture supernatants of hybridomas (purchased from ATCC) and purified using Sepharose 4B Fast Flow Protein G beads for IgG2a antibodies or Protein A beads for IgG1 antibodies. The antibodies were conjugated with Alexa dyes (Alexa 546 and Alexa 647, Thermo Fisher Scientific, Budapest, Hungary) according to the manufacturer's instructions. The dye-to-antibody ratios were in the range of 2.4–3.5 for Alexa 546 conjugated antibodies and between 2.7 and 4.3 for Alexa 647 conjugated antibodies as determined by spectrophotometry. More information can be found in the Supporting Information about how the labeling ratios were determined.

2.3 | Plasmids

*DQA1*0102/pCIneo* and *DQB1*0602/pCIneo* plasmid vectors were kind gifts from Dr. M. A. Kelly, University of Birmingham and Birmingham Heartlands Hospital, Birmingham, UK. Transformation of the plasmids into the DH5α *Escherichia coli* strain and screening with 150 μg/mL ampicillin was performed according to instructions from the Invitrogen manual (Cat. No. 18263-012; Thermo Fisher Scientific). A single colony of transformed *E. coli* was then cultured in 150 mL of Luria Bertani (LB) medium with ampicillin at 200 rpm and 37°C overnight. Cells were incubated until mid-log phase as indicated by the absorbance from 0.4 to 0.7 at 600 nm. Then, an Intron Plasmid Midi kit (Intron Biotechnology, Seongnam-si, South Korea) was used to extract the plasmid. These plasmids were linearized with Xmn1 restriction enzyme (Promega, Madison, WI, USA) and purified by phenol/chloroform extraction.

2.4 | Transfection of the BLS-1 cell line

BLS-1 cells were transfected with *DQA1*0102/pCIneo* and *DQB1*0602/pCIneo* vectors using an Amaxa Nucleofector apparatus (Amaxa, Cologne, Germany). The optimal conditions were established as the X-001 program with Nucleofection C solution using GFP plasmid for electroporation and confocal (fluorescence) microscopy for visual analysis. After electroporation, cells were immediately transferred to 1.5 mL of prewarmed RPMI complete medium and cultured in six-well plates at 37°C for 48 h. Next, the medium was replaced every second day with a stepwise increase in selection drug until 200 μg/mL G418 was reached. The ratio of *DQA1*0102/pCIneo* and *DQB1*0602/pCIneo* plasmids was kept at 1:1, and the resulting cell line was named tDQ6-BLS-1. In addition, cells were transfected with only *DQB1*0602/pCIneo*, and the resulting cell line was named tDQB1-BLS-1.

2.5 | Cell labeling with antibodies

For flow cytometry analysis in each sample, approximately 1 million freshly harvested cells were suspended in 50 μL of phosphate buffered saline (PBS) buffer (pH 7.4) containing 1 mg/mL BSA and 0.01% sodium azide. A saturating concentration of the dye-conjugated antibodies was added to these cells, and the suspension was incubated in the dark for 30 min on ice. After incubation, these cells were washed twice with ice-cold PBS buffer to remove unbound antibodies. Finally, the cells were suspended in 2% formaldehyde solution and kept at 4°C until the measurements were performed in a flow cytometer.

For confocal microscopy, cells were grown on cover slips (12 mm diameter), and after washing with PBS, they were labeled with saturating concentrations of fluorophore-conjugated antibodies (on ice for 30 min) and then washed twice with PBS before fixation with 2% formaldehyde. Finally, coverslips were mounted on microscopic slides using Mowiol 4-88 (Calbiochem, Sigma Aldrich) dissolved in glycerol to avoid photobleaching.

2.6 | Flow cytometry

A FACS Array bioanalyzer (Becton Dickinson, Franklin Lakes, NJ, USA) equipped with 532 and 635 nm lasers were used to study flow cytometric FRET measurements between various epitopes of the cell. In this instrument, donor signals due to 532 nm laser excitation could be collected in the yellow channel through a 585/42 nm bandpass filter, while the acceptor and sensitized acceptor signals on excitation by the 635 and 532 nm lasers could be detected in the red and far-red channels through 661/16 nm bandpass and 685 nm longpass filters, respectively. Data were stored in the FCS 3.0 file format and analyzed for FRET efficiency by ReFlex software (available at https://biophys.med.unideb.hu/en/node/251) [27]. FRET efficiencies were corrected for autofluorescence using mean values of fluorescence intensity distribution histograms of nonlabelled cells, and calculated on a cell-by-cell basis with the display of the mean values of approximately 20.000 cells by the software. The Supporting Information contains examples of original FRET efficiency distribution histograms. From the mean values of six to eight FRET efficiency distribution histograms, we calculated the mean FRET efficiency value with the corresponding SD and displayed as columns on Figure 3.

Sample preparation for standard flow cytometry was performed by using the dye conjugated anti-HLA-DQ antibody, purchased from Becton-Dickinson. JY and nontransfected BLS-1 cell lines were used as positive and negative controls, respectively, for the analysis of HLA-DQ6 expression in tDQ6-BLS-1 cells.

2.7 | Confocal microscopy

A Zeiss LSM 510 confocal laser-scanning microscope (CLSM, Carl Zeiss, Germany) with an adjustable Apochromat ×60 water immersion objective was used to take images of the cells. Excited Alexa 546 and Alexa 647 dye emissions could be detected through 560–605 nm bandpass and 650 nm longpass filters, respectively. Individual cells were selected, and the presence and absence of proteins were determined by detecting the signals in respective photomultiplier tubes.

2.8 | Isolation of RNA from human B lymphocytes

Samples were lysed using TRISOL Reagent (Invitrogen, Thermo Fisher). Total RNA was isolated with chloroform and isopropanol. RNA extracts were dissolved in nuclease-free water (Promega). The concentration and homogeneity of the RNA preparations were determined by measuring the absorbance at 260 and 280 nm with a spectrophotometer (Nanodrop ND1000, Thermo Fisher). Standardized amounts of RNA were then digested with DNase (Ambion, Thermo Fisher) and subjected to reverse transcription using Super Script II RNase H-Reverse Transcriptase and Random Primers (Invitrogen, Thermo Fisher). Reverse transcription of 50 ng of total RNA was performed at 42°C for 60 min and at 72°C for 5 min.

2.8.1 | TaqMan real-time reverse transcription polymerase chain reaction

Quantitative real-time analyses were performed in 96-well optical reaction plates in an ABI Prism 7700 sequence Detector (Applied Biosystems, Thermo Fisher). All oligo mixes were purchased from ABI. Taq DNA Polymerase (Fermentas, Burlington, Ontario, Canada) was used for amplification, and Rox Reference Dye (Invitrogen, Thermo Fisher) was used for normalization of the fluorescent reporter signal. Amplification was conducted in a 25 µL reaction mixture containing 125 ng of cDNA. All PCRs were performed in duplicate for each cDNA product. We used the following conditions: 40 cycles at 95°C for 12 s and 60°C for 30 s. The real-time PCR data were developed by using Sequence Detector System version 2.1 software (Applied Biosystems, Thermo Fisher). The expression levels were calculated by a comparative threshold cycle (ΔC_t) method. The number of targets was normalized to the human 36B4 housekeeping gene as an endogenous control.

2.9 | Immunogold labeling and transmission electron microscopy experiments

TEM was used to study the membrane protein patterns on the nanometer and micrometer scale on the immunogold-labeled samples. Freshly harvested cells (1×10^6 cells) were washed twice in ice-cold PBS (pH 7.4). Cell surface proteins (HLA I or II) were labeled with 50 µg/mL primary mAbs for 40 min on ice. Thereafter, the cells were washed in PBS and labeled with secondary antibodies conjugated to 15 nm diameter colloidal gold beads (AuroProbe EM 15 nm, Amersham Pharmacia, Little Chalfont, UK). The cells were washed three times. After appropriate labeling with primary and secondary antibodies, the cells were fixed with 2% paraformaldehyde. Gold beads of different sizes carrying anti-mouse polyclonal antibody coatings were added after the monoclonal antibody treatments. Alternatively, to investigate the surfaces of whole cells, cells were sedimented onto poly-L-lysine-treated Collodium grids. Cells were dehydrated with a graded ethanol series consisting of the following concentrations of ethanol: 10% for 3 min, 30% for 3 min, 50% for 3 min, 70% for 3 min, and 95% for 5 min. Samples were critical point dried (Quorum Technologies, E3000, Jyväskylä, Finland). The loading of the grid into the sample holder and into the chamber of the critical point dryer was done under ethanol to prevent air-drying of the samples. The chamber was sealed and cooled to 18°C. The ethanol in the chamber was replaced with liquid CO_2 via a series of fluid exchanges. Each fluid exchange consisted of a 1-min flush of the chamber with liquid CO_2 followed by a 5-min immersion in CO_2 with no flow. The CO_2 fluid level was adjusted so that the sample holder remained submerged at all times. After the removal of the ethanol, the chamber was heated to the critical point of CO_2 (31°C, 73 atm), and the chamber was depressurized over a period of 5 min. Then, we decreased the pressure at a constant temperature (40°C). The dry samples were stored in a desiccator prior to imaging to prevent the absorption of water from the air [28]. Next, the critical point-dried whole cell samples were coated with a thin layer of amorphous carbon using an electron beam carbon evaporator. The carbon deposition rate was 20 nm thick. After coating, we dissolved the Collodium with amyl acetate (Sigma), washed it with acetone and then kept the samples in alkaline lysis buffer (1% lauryl sulfate, 2.5 M NaCl, 10 mM Tris, NaOH, 100 mM EDTA, pH 10, 100 mL DMSO (10%, 1.28 M), 10 mL Triton-x-100 [1%, 16 mM]), washed them with water, and dried them at room temperature. TEM was performed by a JEOL2000 FX-II instrument (JEOL, Tokyo, Japan) operated at 120 kV.

2.10 | ClickOnGold

We implemented an image processing algorithm to localize electron-dense areas/gold beads on electron micrographs. An image processing program named "ClickOnGold" was developed. During image analysis, we modify the picture by performing operations on it to separate the important piece of information from the background. Image processing/image analysis can be performed by many possible methods, which lead to different results, but we will discuss only convolution and periphery discrimination since the "ClickOnGold" program uses these operations in the process of image analysis [29]. The "ClickOnGold" program is available free of charge from the following website: https://biophys.med.unideb.hu/sites/default/files/file_uploads/clickongold.zip

2.11 | Statistical analysis

2.11.1 | Flow cytometry

For comparison, either an unpaired t test or one-way ANOVA together with Tukey post hoc analysis was performed using SigmaStat 3.5 (GmbH, Germany) depending on the number of groups. Only "*p*" values <0.05 were considered significant. Nonsignificant "*p*" values are indicated by the abbreviation "N.S.," whereas "*p*" values <0.05, <0.01, and <0.001 are denoted with *, **, and ***, respectively, in the figures.

2.11.2 | Transmission electron microscopy

For the evaluation of the TEM images, we used the pair correlation function (PCF). This is a powerful tool for describing the point pattern property of antigens on the cell surface (gold beads). The method is based on Ripley's K function [30, 31]. After we determined the position (i.e., the coordinates) of the beads with "ClickOnGold" software from the TEM images, we applied Gold software, which can calculate the magnitudes of PCFs with Monte Carlo simulations [32, 33]. This software defines the PCF values of the point pattern and additional upper and lower 95% confidence intervals. If the PCF value is larger than the upper limit, the pattern is aggregated; if lower, it is segregated. Between the limits, the points have a random distribution. Furthermore, the peaks of the PCF provide information on the numbers of clusters having defined sizes.

3 | RESULTS

3.1 | Expression of HLA-DQ6 in human B lymphocyte cell lines

First, we aimed to confirm the expression of HLA-DQ6 (MHC class II) in different human B lymphocyte cell lines. To verify the gene expression of the beta chain of HLA-DQ6, we determined HLA-DQB1 mRNA expression using Q-RT-PCR in the nonmanipulated controls (BLS-1), in JY cells (endogenously expressing HLA-DQ6) and in cells that were transfected either with beta chain-coding (tDQB1-BLS-1) or with alpha plus beta chain-coding (tDQ6-BLS-1) plasmids. Our results show that while the JY cell line strongly expresses HLA-DQB1 mRNA, the expression of this mRNA is not detectable in BLS-1 cells, as previously described in the literature (Figure 1A) [25, 26]. Although the expression level of HLA-DQB1 mRNA was different in tDQB1-BLS-1 cells from that of tDQ6-BLS-1 cells, these expression levels are both significantly higher than that of the BLS-1 cells.

To prove that the cotransfection of DQA1 (alpha chain) and DQB1 (beta chain) indeed results in the cell surface appearance of HLA-DQ6 protein, we carried out flow cytometric analysis using anti-HLA-DQ antibodies. As the histogram shows, we detected strong fluorescence intensity in the case of tDQ6-BLS-1 cells, in contrast to BLS-1 or tDQB1-BLS-1 cells, where the fluorescence signals were not significantly higher than the background intensity of the unlabeled cells (Figure 1B,C).

The distribution pattern of HLA-DQ6 protein in the tDQ6-BLS-1 cell membrane was also verified by CLSM. The blue pixels on the microscopic images indicate that HLA-DQ6 proteins localize in disperse patches on the cell surface (Figure 1D). A similar distribution pattern was detected on JY cells.

These results together show that following DQ6 transfection, tDQ6-BLS-1 cells express DQ6 (HLA class II) at both the mRNA and protein levels, and protein expression was detectable on the cell surface.

3.2 | Expression and transcription of HLA-B in transfected BLS-1 cells

To characterize HLA I expression in the abovementioned B lymphocyte cell lines, we first measured HLA-B mRNA expression using Q-RT-PCR. We found that JY cells expressed the highest amount of HLA-B mRNA, while BLS-1 cells expressed the lowest amount of HLA-B mRNA among these cells. The expression level of HLA-B mRNA in tDQB1-BLS-1 cells was similar to that in BLS-1 cells, whereas the expression level of HLA-B mRNA in tDQ6-BLS-1 cells was more than twofold higher than that in BLS-1 cells but only half of that in JY cells (Figure 2A).

Next, we measured the cell surface expression of HLA I proteins by flow cytometry using a W6/32 antibody that recognizes a common epitope of HLA-A, -B, and -C proteins. We detected relatively low cell surface expression of HLA I proteins in BLS-1 cells, while it was two times higher in JY and tDQB1-BLS-1 cells and four times higher in tDQ6-BLS-1 cells (Figure 2B). This tendency correlates with the results obtained using the Q-RT-PCR method.

These results show that the expression of HLA-DQ6 and even the transfection of BLS-1 cells with only *DQB1*0602/pCIneo* affect the expression of HLA class I molecules, although in the latter case, HLA-DQ molecules were not present on the cell surface (Figure 1C).

3.3 | The effect of HLA-DQ6 cell surface expression on the homoassociation of HLA and ICAM-1 molecules

It has been reported that membrane proteins of immune synapses localize in lipid rafts, and the appearance of a newly synthesized protein in the membrane tends to strongly affect not only the distribution and localization of other proteins but also their association with each other [34, 35]. We hypothesize that the inclusion of HLA-DQ6 in the membrane of the cells will influence the distribution of nearby molecules such as HLA I and ICAM-1 molecules since they are often found in immune synapses.

To assess how the appearance of HLA-DQ6 molecules in the cell membrane influences the cell surface distribution pattern of

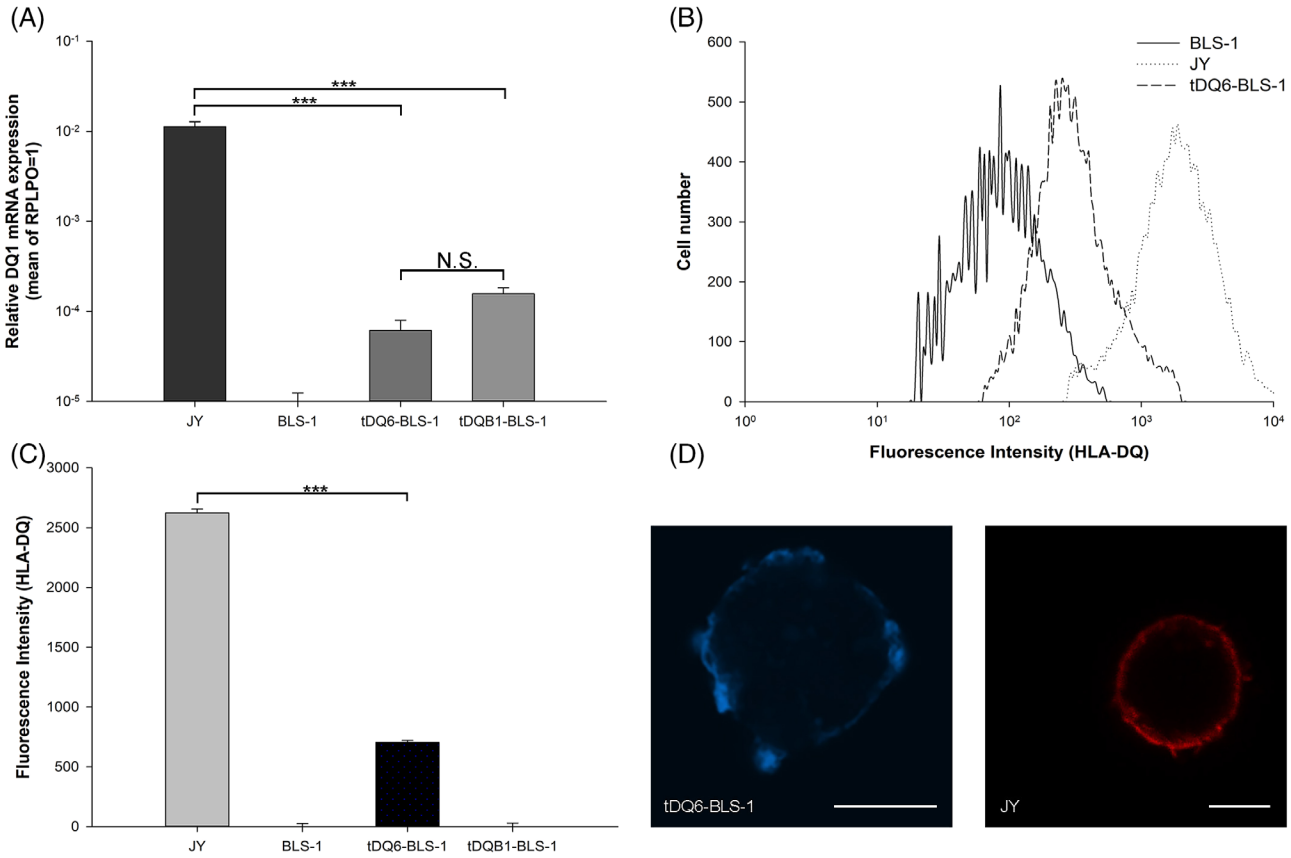

FIGURE 1 Transcription and expression of HLA-DQ6 on human B lymphocyte cell lines. (A) The transcription profile of HLA-DQB1 mRNA in human B lymphocytes was detected by quantitative PCR (Q-RT-PCR). Total RNA was extracted and processed as described in Section 2. The relative amount of HLA-DQB1 (beta chain-coding) transcripts was normalized to the human 36B4 housekeeping gene. Data shown are the means ± SDs of triplicate measurements. "N.S." indicates a nonsignificant "*p*" value, whereas "*p*" value <0.001 is denoted with ***. (B) Cell surface expression of the transfected HLA-DQ6 protein demonstrated by flow cytometry. Flow cytometric intensity histograms of control, nontransfected, HLA II-deficient (BLS-1) and transfected cells (tDQ6-BLS-1) were labeled (1×10^6 cells) with an Alexa 546-conjugated anti-HLA-DQ/DR monoclonal antibody. The mean values of the fluorescence intensity histograms were background corrected. The histograms contain data from approx. 20,000 cells (Continuous line: BLS-1 cells, dashed line: transfected cells (tDQ6-BLS-1), dotted line: JY cells). (C) Mean values of the histograms shown in Figure 1B are plotted. The expression level of HLA-DQ was significantly higher at the JY cell surface than at the surface of tDQ6-BLS-1 cells. The fluorescence signal of BLS-1 or tDQB1-BLS-1 cells was practically the same as the background intensity of the unlabeled cells. Data shown are the means ± SDs of triplicate measurements. A "*p*" value <0.001 is denoted with ***. (D) HLA-DQ6 protein cell surface expression on transfected tDQ6-BLS-1 and JY human B cells. Cells were labeled with Alexa 647 (blue color, tDQ6-BLS-1) and Alexa 546 (red color, JY) dye-conjugated anti-HLA-DQ antibodies and analyzed by confocal laser scanning microscopy. The bars represent 5 μm. [Color figure can be viewed at wileyonlinelibrary.com]

HLA I and ICAM-1 membrane proteins, we used flow cytometric FRET experiments. We studied the homo and heteroassociation patterns of HLA I, HLA II and ICAM-1 on the abovementioned B-cell lines.

Our results show significant homoassociation between HLA I heavy chain (HLA I-HC) molecules in BLS-1 cells expressing only HLA I (supported by the high FRET efficiency of 27%) and stronger homoassociation in JY cells that express both HLA I and HLA II as well (FRET efficiency ~37%; Figure 3A). The de novo expression and appearance of HLA-DQ6 in tDQ6-BLS-1 cells reduced the homoassociation between HLA I-HC. Similarly, the transfection of BLS-1 cells with *DQB1*0602/pCIneo* reduced the homoassociation between HLA I-HC (FRET efficiency was only ~10% in both cases). This observation was interesting, since in these cases, the cell surface expression of HLA I molecules was higher in tDQ6-BLS-1 cells and in tDQB1-BLS-1 cells than in the parent BLS-1 cells.

In the case of HLA I light chain (i.e., β_2 microglobulin, HLA I-LC), we observed a tendency similar to that of HLA I-HC (data not shown).

The homoassociation of HLA II molecules was significantly higher on tDQ6-BLS-1 cells than on JY cells. The lack of cell surface expression of HLA II molecules on BLS-1 and tDQB1-BLS-1 cells prevented FRET measurements in these cell lines (Figure 3A).

While ICAM-1 homoassociation was low in JY cells, the FRET efficiency and therefore the homoassociation between ICAM-1 was higher in BLS-1 cells and further increased in tDQ6-BLS-1 and tDQB1-BLS-1 cells (Figure 3A).

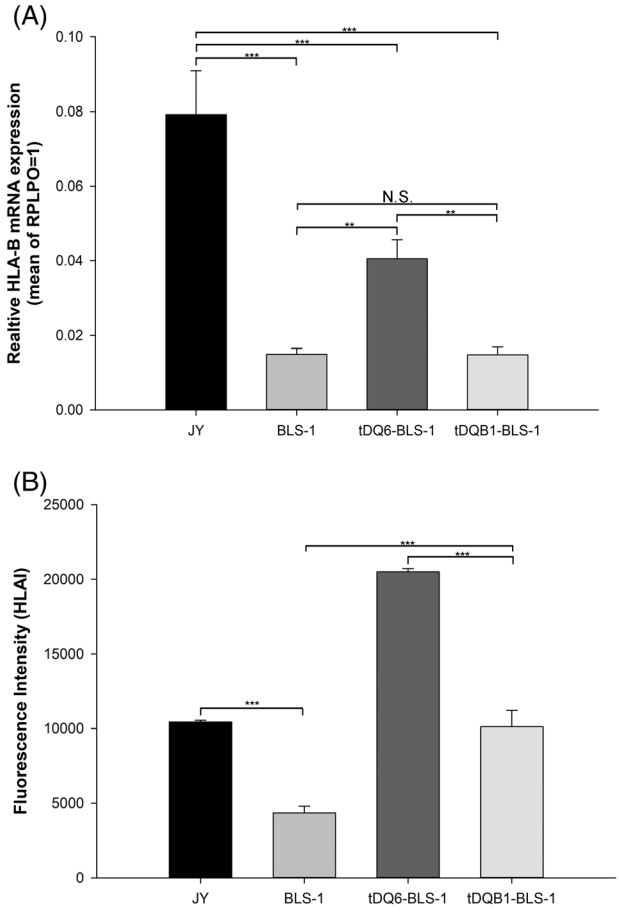

FIGURE 2 Transcription and expression of HLA I on human B lymphocyte cell lines. (A) The transcription profile of HLA-B mRNA in human B lymphocytes was detected by quantitative PCR. Real-time qPCR analysis of HLA-B mRNA expression relative to h36B4 mRNA levels in transfected and nontransfected B lymphocytes is shown in the charts. Data represent the mean ± SD of a triplicate experiment. The experiment was repeated in an independent set of lymphocytes with similar results. A "*p*" value <0.01 is denoted with **, and "*p*" <0.001 with ***. (B) The cell surface expression profile of human leukocyte antigen heavy chain (HLA I-HC) on human B lymphocytes was detected by flow cytometry. In our experiments, we used a monomorphic W6/32 (anti-HLA-A, -B, -C) monoclonal antibody labeled with Alexa 546. The columns are the mean values of fluorescence intensity distribution histograms of triplicate measurements. The error bars represent SD. A "*p*" value <0.001 is denoted with ***.

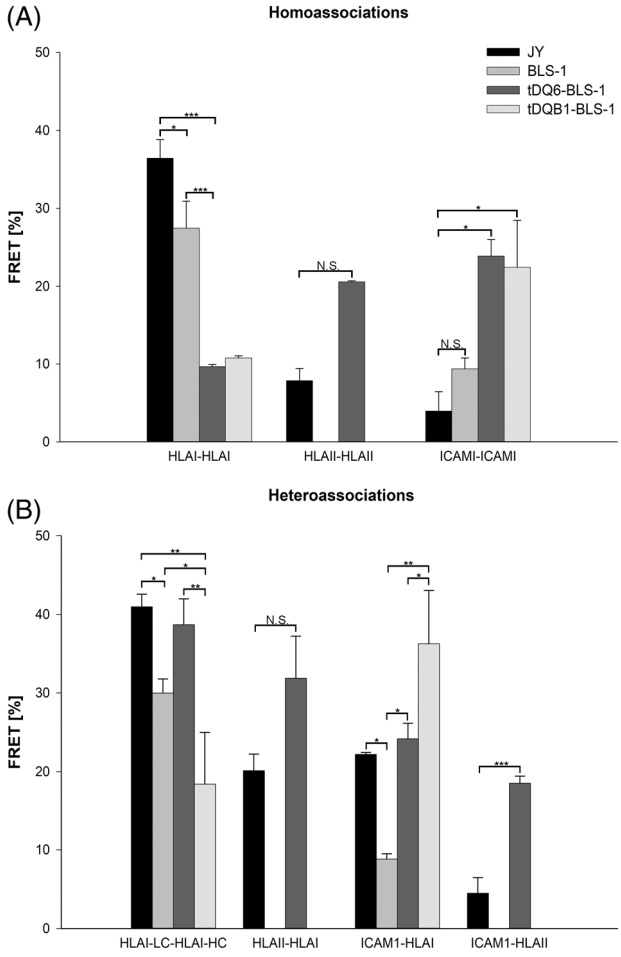

FIGURE 3 Effect of HLA-DQ6 cell surface expression on the homo and heteroassociation of HLA and ICAM-1 molecules. (A) FRET efficiency of homoassociation of HLA I, HLA II, and ICAM molecules on B-cell lines. The calculated FRET values are presented as comparative bar diagrams. FRET efficiency was measured between monoclonal antibodies directed against epitopes on JY, BLS-1 and tHLA-DQ6-BLS-1 and tDQB1-BLS-1 cell lines. Flow cytometric FRET measurements were performed on cells simultaneously labeled with Alexa Fluor 546- and Alexa Fluor 647-conjugated monoclonal antibodies. FRET efficiency was calculated on a cell-by-cell basis, and for the resulting FRET efficiency distribution histograms, the mean values were determined from 3 to 6 parallel measurements and are shown as the mean ± SD. "N.S." indicates a nonsignificant "*p*" value, whereas "*p*" values <0.05 and <0.001 are denoted with * and ***, respectively. (B) FRET efficiency of heteroassociation between HLA I light chain (β_2-microglobulin, HLA I-LC) and HLA I heavy chain (HLA I-HC), HLA II and HLA I, ICAM 1 and HLA I, and ICAM 1 and HLA II on B-cell lines. Fluorescence resonance energy transfer was measured between donor- and acceptor-labeled monoclonal antibodies. The first protein was labeled with a donor-conjugated antibody, and the second protein was labeled with an acceptor-conjugated antibody. The monoclonal antibody W6/32 labels all HLA-A, HLA-B, and HLA-C molecules, and the β_2-microglobulin-specific L368 antibody labels all the class I molecules associated with the light chain, that is, β_2-microglobulin. The anti-HLA-DQ recognizes all of the DQ molecules, and the P2A4 monoclonal antibody labels the ICAM-1 molecules. FRET efficiency was calculated on a cell-by-cell basis, and from the resulting FRET efficiency distribution histograms, the mean values were determined from 3 to 6 parallel measurements and are shown as the mean ± SD. "N.S." indicates a nonsignificant "*p*" value, whereas "*p*" values <0.05, <0.01, and <0.001 are denoted with *, **, and ***, respectively.

3.4 | Effect of HLA-DQ6 cell surface expression on the heteroassociations of HLA and ICAM-1 molecules

Since we have seen significant changes in the homoassociations of HLA and ICAM-1 molecules, we sought to further analyze whether heteroassociations between these molecules are affected by the de novo expression of HLA-DQ6.

High intramolecular FRET efficiency was measured between HLA I-LC and HLA I-HC on JY cells, while it was weaker in the case of BLS-1 cells (Figure 3B). The expression of HLA-DQ6 significantly induced heteroassociation between the two chains of HLA I, and the

FRET efficiency increased to the level measured in JY cells. The heteroassociation between HLA I-LC and HLA I-HC decreased in the tDQB1-BLS-1 cells (Figure 3B).

Heteroassociation was also detected between the HLA-II and HLA I-HC proteins on JY cells. The association between these proteins in BLS-1 and tDQB1-BLS-1 cells was not detectable since these cells do not express HLA II proteins on the cell surface. However, a detectable association was measured between HLA-II and HLA I-HC in the HLA-DQ6-expressing tDQ6-BLS-1 cells, and the FRET efficiency was even higher than that measured in JY cells, although this increase did not reach a statistically significant level (Figure 3B).

Heteroassociation was also detected between the ICAM-1 and HLA I-HC proteins on JY cells (FRET efficiency ~23%). The heteroassociation between these proteins in BLS-1 cells was lower, as demonstrated by the much lower FRET efficiency (~8%). However, a significantly higher association was measured between ICAM-1 and HLA I-HC in HLA-DQ6-expressing tDQ6-BLS-1 cells. This heteroassociation between ICAM-1 and HLA I-HC was slightly more elevated than that on JY cells (FRET efficiency ~25%). The ICAM-1 and HLA I-HC heteroassociation was even higher in the tDQB1-BLS-1 cells (Figure 3B).

The level of heteroassociation between ICAM-1 and HLA-II was much lower on JY cells (FRET efficiency ~5%). However, a significantly higher association was measured between ICAM-1 and HLA-II in the HLA-DQ6-expressing tDQ6-BLS-1 cells (FRET efficiency ~25%; Figure 3B).

These data suggest that with the help of transfection, the previously unmanifested DQ6 cell surface molecule is able to integrate into protein clusters, changing the already existing cell surface pattern. The expression of DQ6 will often shift the association tendency toward that in the control JY cells. The newly appearing molecules on the cell surface are able to integrate within proximity to other molecules and therefore can influence the previously existing molecular distribution pattern.

3.5 | The cell-surface pattern changes on a higher hierarchical level

As the results obtained from FRET studies suggested a modified cell surface distribution pattern of HLA proteins, we aimed to study the membrane topology of HLA I and HLA II molecules on a submicrometer scale using TEM. To visualize different molecules per cluster, we used the immunogold labeling method, which provides information about molecular patterns between 20 nm and a micrometer scale.

Here, we directly measured the distribution of HLA I and HLA II clusters at this hierarchical level in the plasma membrane of the three different cell lines (JY, tDQ6-BLS-1, BLS-1) using gold labels. Both HLA I and HLA II molecules were labeled by antibodies conjugated with 10, 20, or 30 nm gold beads. The distribution of gold nanoparticles on TEM micrographs (Figure 4A,B,C,G,H,I) was analyzed by "ClickOnGold" software [29]. The corresponding PCFs are shown in Figure 4D,E,F,J,K. The analysis of PCF shows that in the case of JY cells, the distribution of HLA I molecules in the 10–20 nm and the 20–50 nm distance ranges are significantly different from the values determined assuming random distribution (Figure 4A,D). HLA II molecules also showed nonrandom distribution on JY cells, according to the PCF function clusters of HLA II molecules detected in the 10–20, 30–150, and 190–210 nm ranges (Figure 4B,E). In BLS-1 cells, HLA I molecules demonstrated nonrandom distribution in the 10–20 nm, 30–120 nm, and slightly in the 210–350 nm distance ranges according to the PCF function (Figure 4B,E). BLS-1 cells did not express HLA II molecules on the cell surface (Figure 4H, negative control), so PCF analysis was not performed. In tDQ6-BLS-1 cells, the expression of HLA I molecules showed a nonrandom distribution in the 10–210 nm range (Figure 4C,F), and newly synthesized HLA II (HLA-DQ) appeared on the cell surface, forming clusters in the 10–200 nm and 400–600 nm ranges (Figure 4I,K). The de novo synthesized HLA-DQ molecules definitely showed nonrandom characteristic properties on this hierarchical level.

We also wanted to see whether the HLA I and HLA II clusters are separated or interspersed on the cell surface. Therefore, we performed double immunogold labeling on JY and tDQ6-BLS-1 cells using antibodies against HLA I and HLA II molecules conjugated to 10 and 20 nm gold beads, respectively. Figure 5A,B shows micrographs of JY and tDQ6-BLS-1 cells, respectively. From several of these types of micrographs, the PCFs were determined for HLA I (Figure 5C,D) and HLA II molecules (Figure 5E,F), and the pair cross-correlation functions (PCCFs) were calculated (Figure 5G,H). On JY cells, the PCF of HLA I molecules showed possible clusters in the 200 nm range (Figure 5C), and the PCF of HLA II molecules indicated HLA II clusters between the 20 and 200 and between the 300 and 380 nm ranges (Figure 5E). The PCCF of HLA I and HLA II molecules indicated a mild association between HLA I and HLA II molecules at approximately 25, 75, and 175 nm (Figure 5G). It should be noted that some of the peaks are barely above the 95% significance level therefore the interpretation of these associations should be considered with caution. On tDQ6-BLS-1 cells, the PCF of HLA I molecules showed possible clusters around the 20–60 nm range (Figure 5D), and the PCF of HLA II molecules indicated HLA II clusters of approximately 60 and 600 nm (Figure 5F). In contrast to the JY cells, the PCCF of HLA I and HLA II molecules on tDQ6-BLS-1 cells showed no measurable association between HLA I and HLA II molecules (Figure 5F), indicating that in these cells, the de novo synthesized HLA DQ molecules do not intersperse with HLA I clusters.

4 | DISCUSSION

MHC class I and II molecules play essential roles in antigen presentation to T lymphocytes. Antigen presentation by MHC class II is essential for the activation of CD4 T cells, whereas MHC class I molecules are required for the activation of CD8 T cells [4]. Both MHC class I and class II molecules are highly inducible, and their expression is crucial for the induction and maintenance of adaptive immune responses presenting endogen-originated antigens to CD8+ T lymphocytes. In

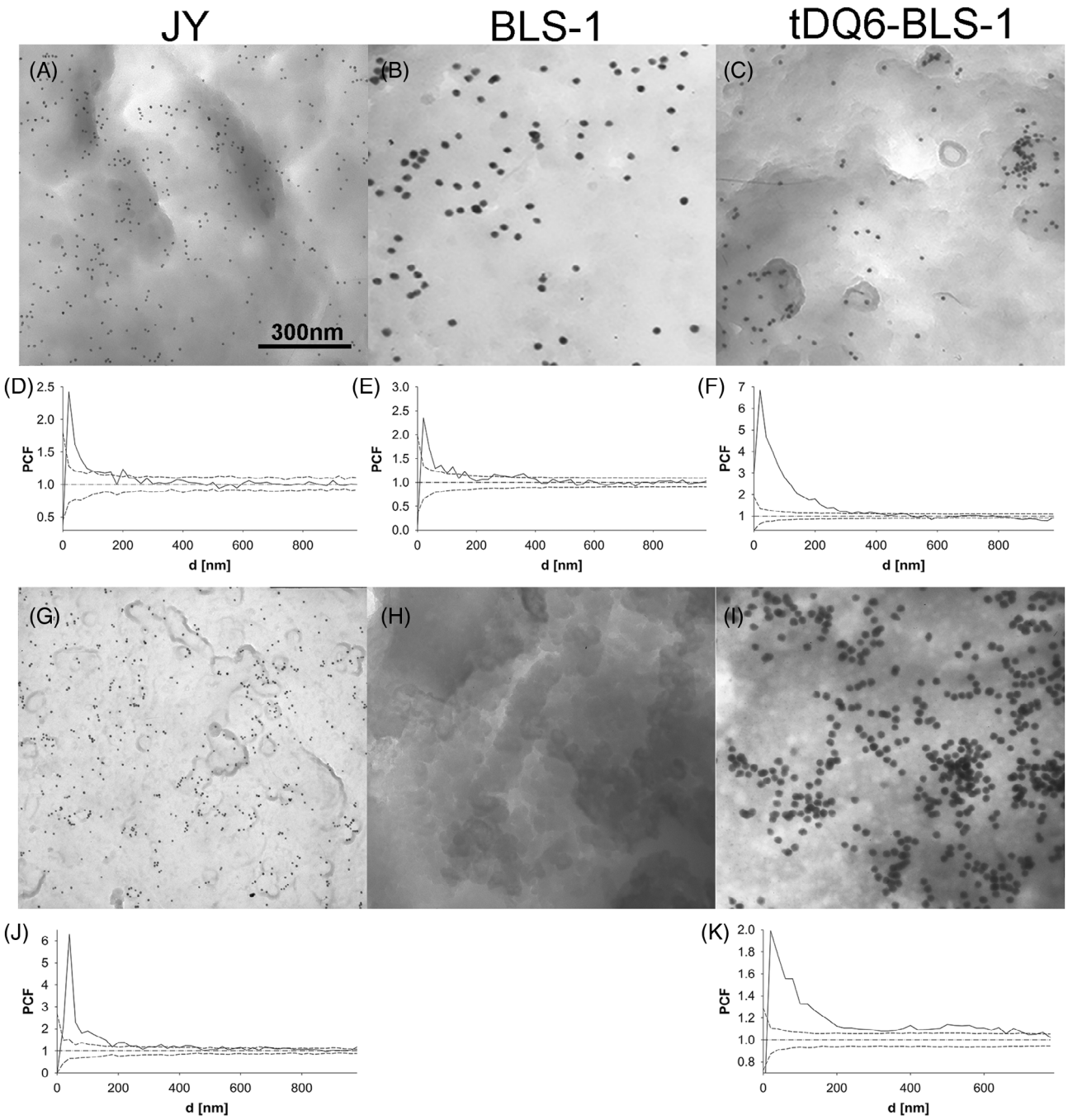

FIGURE 4 Immunoelectron microscopy of HLA I and II molecules on JY, BLS-1, and tDQ6-BLS-1 cells. HLA I and HLA II molecules of transfected and nontransfected cells were labeled with anti-HLA I (W6/36) and anti-HLA II (anti-HLA-DQ) primary monoclonal antibodies and then with secondary antibodies conjugated to 10, 20, or 30 nm diameter colloidal gold nanoparticles as described in Section 2. After fixation, we sedimented the labeled cells onto poly-L-lysine-treated Collodium grids. After drying at the critical point, whole cell samples were coated with carbon. We dissolved the Collodium and denatured the proteins and the DNA with alkaline lysis buffer. After drying, the samples were analyzed with electron microscopy at 120 kV. The scale bar is 300 nm and is valid for all micrographs. (A) HLA I (10 nm) was labeled on JY; (B) HLA I (30 nm) was labeled on BLS-1, (C) HLA I (20 nm) was labeled on tDQ6-BLS-1 cells. The corresponding pair correlation functions (PCFs) are (D) HLA I on JY cells, (E) HLA I on BLS-1 cells, and (F) HLA I on tDQ6-BLS-1 cells. (G) HLA II (10 nm) was labeled on JY; (H) HLA II (30 nm) was labeled on BLS-1 cells, serving as a negative control; (I) HLA II (30 nm) was labeled on tDQ6-BLS-1 cells. The corresponding PCFs are (J) HLA II on JY cells and (K) HLA II on tDQ6-BLS-1 cells. On the PCF graphs, the continuous line represents the calculated PCF, the dotted dashed line is the value 1, and the upper and lower dashed lines represent the range of random distribution.

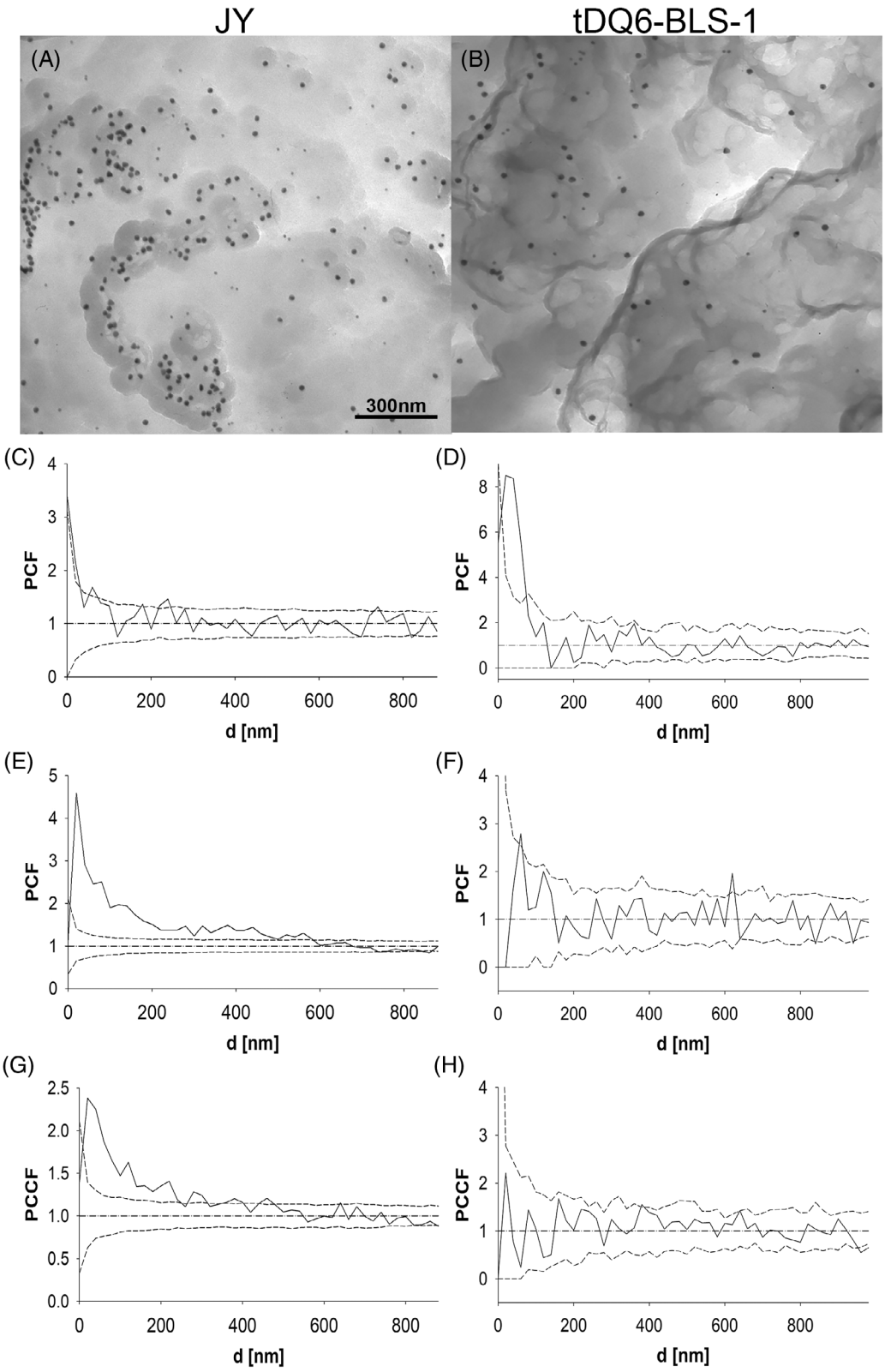

FIGURE 5 Legend on next page.

addition to their key role in antigen presentation, MHC I molecules also participate in the regulation of several signal-transmitting processes affecting cell growth and differentiation [36].

Autoimmune diabetes, also known as type 1 diabetes mellitus (T1DM), is typically characterized by the autoimmune destruction of the insulin-producing β-cells of the pancreas, which results in a

shortage of insulin and therefore disturbs the regulation of anabolism and catabolism. It shows an association with class II HLA loci (especially with *HLA-DRB1*04-DQB1*0302* and *HLA-DRB1*03-DQB1*0201*). The HLA-DQ6 allele as a defense against T1DM is well established [14]. To study the effect of the expression of DQ molecules on the cell surface distribution of other membrane proteins, we selected the HLA class II-negative BLS-1 cell line isolated from patients with BLS [25, 37]. We followed the earlier paper by Kelly et al. to establish the stably transfected BLS-1 cell line, tDQ6-BLS-1, expressing DQ molecules [37]. Since HLA I, HLA II, and ICAM-1 are randomly distributed and often colocalized in the cell membrane, we expected the de novo synthesized HLA-DQ6 molecule in tDQ6-BLS-1 to integrate and form clusters with the HLA I and ICAM-1 molecules on the cell surface [23, 24, 38–42]. We wondered whether these clusters at the tD6-BLS-1 cell membrane are different from those at the parent BLS-1 cell line and from those of the JY cell line (which expresses HLA class I, class II, and ICAM-1 molecules). To address these questions, we first characterized the tDQ6-BLS-1 cell line and determined that tDQ6-BLS-1 cells express DQ6 at both the mRNA and protein levels using Q-RT-PCR and immunofluorescence, respectively (Figure 1). We also investigated the effect of transfection on the expression level of HLA class I molecules and determined that HLA class I expression was induced by transfection at both the mRNA and protein levels. Interestingly, this phenomenon was also observed even in the tDQB1BLS-1 cells, where the DQ molecules were not expressed on the cell surface, although the mRNA coding for half of the DQ molecules was present (Figure 2). The reason for this induction is not known; it is possible that the transfection enhanced HLA I processing, resulting in higher cell surface expression.

Next, we wanted to study the cell surface distribution of these molecules using FRET to reveal molecular associations within the 10 nm level and to characterize cluster formation using TEM approaches at higher hierarchical levels between the 20 nm and submicrometer levels.

First, we studied the homoassociation of HLA class I, class II, and ICAM-1 molecules. High FRET efficiency was detected between HLA class I molecules on JY and BLS-1 cells, and much lower FRET efficiency was measured on the tDQ6-BLS-1 and tDQB1-BLS-1 cells, although the expression level of HLA class I molecules was significantly higher on these cells than on the parent BLS-1 cells (Figures 2 and 3). When we talk about "high" and "low" FRET efficiency we have to consider the following. The FRET efficiency depends not only on the distances between the donor and acceptor molecules, but also on the fact that not all donor molecules are the FRET distance so there are orphan donor molecules with zero FRET efficiency. We measure the average ensemble FRET efficiency coming from all molecular species on the cell surface labeled with the appropriate donor and acceptor fluorophores therefore the ensemble FRET efficiency on a single cell depends on both the distances and the relative concentrations. According to our judgment, the distances do not change to much within the associated molecules but rather the proportion of the molecules which are associated or not associated. So, the observation that the FRET efficiency was lower on the tDQ6-BLS-1 and tDQB1-BLS-1 cells than on the parent BLS-1 cells, although the expression level of HLA class I molecules was significantly higher on these cells than on the parent BLS-1 cells suggests that the newly appearing HLA class I molecules go to the cell surface mostly as monomers. FRET studies showed significantly higher homoassociation between HLA class II molecules on tDQ6-BLS-1 than on JY cells, although the expression level of HLA class II molecules was five times higher on JY cells, suggesting that the de novo synthesized DQ molecules go to the cell surface in associated states (mostly as dimers or higher oligomers). Similarly, higher homoassociation was detected between ICAM-1 molecules on the tDQB1-BLS-1 and tDQB1-BLS-1 cells than on the JY or on the parent BLS-1 cells. This can be explained only if we consider that the ICAM-1 molecules can associate with the HLA class I and class II molecules as well. Homoassociations do not exist in a "clear" form, and the presence of other proteins in these protein complexes cannot be excluded; therefore, we aimed to study the heteroassociations between these proteins.

As expected, high energy transfer was measured between the HLA class I light chain and HLA class I heavy chain in all cell lines. However, the FRET efficiency value was somewhat lower on the parent BLS-1 and the tDQB1-BLS-1 cells. This observation can be deciphered only by using antibodies binding to the free heavy chains of HLA class I molecules, which was beyond the scope of this study. The heteroassociation between HLA class II and HLA class I molecules was somewhat higher on tDQ6-BLS-1 cells than on JY cells, although the increase did not reach the significance level. A higher degree of heteroassociation was detected on tDQ6-BLS-1 and tDQB1-BLS-1 cells than on the parent BLS-1 cells, probably because the induced HLA I expression brought along ICAM-1 molecules as well. Similarly, a higher level of heteroassociation was detected between ICAM-1 and HLA class II molecules on tDQ6-BLS-1 cells than on JY cells, probably because the de novo synthesized DQ molecules could bring along ICAM-1 molecules or preferentially associate with already existing ICAM-1 molecules on the cell surface. These phenomena could explain why the homoassociation of ICAM-1 molecules was so high on the transfected tDQ6-BLS-1 and tDQB1-BLS-1 cells (Figures 2 and 3).

FIGURE 5 Transmission electron microscopy (TEM) micrographs of double immunogold-labeled HLA I and HLA II molecules on JY and tDQ6-BLS-1 cells. Samples were labeled with anti-HLA I and anti-HLA II antibodies conjugated with 10 and 20 nm beads. The labeling procedure was similar to that described in Figure 4 legend. (A) TEM micrographs of HLA I (10 nm) and HLA II (20 nm) on JY cells. The scale bar is 300 nm, which is valid for panel B as well. (B) TEM micrographs of HLA I (10 nm) and HLA II (20 nm) on tDQ6-BLS-1 cells. The corresponding pair correlation functions (PCFs) are (C) HLA I on JY cells; (D) HLA I on tDQ6-BLS-1 cells; (E) HLA II on JY cells; and (F) HLA II on tDQ6-BLS-1 cells. The pair cross-correlation function (PCCF) indicates the cross-correlation function of HLA I and HLA II. (G) PCCF of HLA I and HLA II on JY cells; (H) PCCF of HLA I and HLA II on tDQ6-BLS-1 cells. On the PCF and PCCF graphs, the continuous line represents the calculated PCF or PCCF, the dotted dashed line is the value 1, and the upper and lower dashed lines represent the range of random distribution.

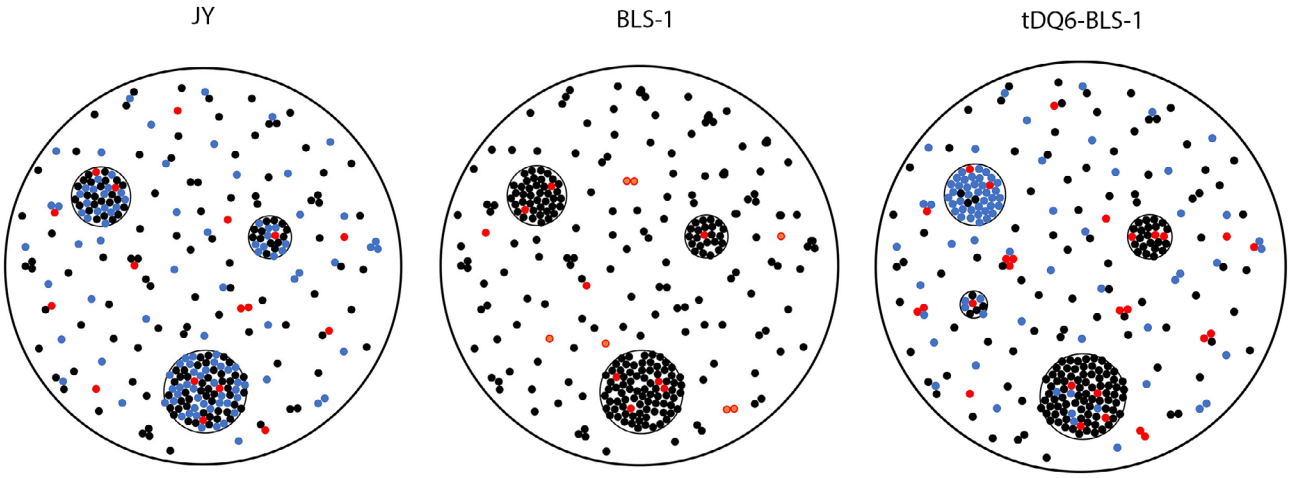

FIGURE 6 Possible distribution of cell surface proteins on JY, BLS-1, and tDQ6-BLS-1 cells based on FRET and electron microscopic measurements. Cell surface distribution of HLA I (black dots), HLA II (blue dots), and ICAM-1 (red dots) molecules. BLS-1 cells have no HLA II molecules on the cell surface. Note that on the tDQ6-BLS-1 cells where we reintroduced the HLA II (DQ) molecules, the de novo synthesized DQ clusters did not mix with HLA I clusters. [Color figure can be viewed at wileyonlinelibrary.com]

After the detailed FRET studies, we investigated the cell surface topology of HLA class I and HLA class II molecules on the submicrometer scale using a TEM approach on the JY, BLS-1, and tDQ6-BLS-1 cells. Using antibodies conjugated to various sizes of gold beads, we were able to show that HLA class I and class II molecules were unevenly distributed in the TEM micrographs of JY and tDQ6-BLS-1 cells, where they formed clusters of various sizes. Understandably, the parent BLS-1 cells have only HLA class I clusters because HLA class II molecules were absent in this cell line. The sizes of these clusters were determined from PCFs (Figure 4).

Using double immunogold labeling on JY and tDQ6-BLS-1 cells, we wanted to see whether the HLA class I and class II clusters are interspersed or separated. The pair cross-correlation function showed that on JY cells, the HLA class I and class II molecules are mixed and interspersed in the clusters. We were also able to detect HLA class I and class II clusters on tDQ6-BLS-1 cells, but these clusters were separated. The de novo synthesized DQ molecules form separated clusters on the cell surface, and they do not intermingle with HLA class I clusters (Figure 5.)

Combining our FRET and TEM data, we were able to suggest a model for the cell surface distribution of HLA class I, class II, and ICAM-1 molecules (Figure 6). In the case of JY cells, HLA class I and class II molecules form coclusters within which even ICAM-1 molecules can be found. FRET can be measured between these molecules within the clusters and outside clusters, indicating homo and heteroassociations between these molecules. In the case of tDQB6-BLS-1 cells, HLA class I and class II molecules form separate clusters. FRET values monitoring homoassociations can come from both the clusters and from outside of clusters, but FRET values monitoring heteroassociations can come mostly from outside of clusters. Most likely, it takes a longer time for the independent HLA class I and class II clusters to intermingle, potentially weeks, or months. The parent BLS-1 cells have only HLA class I clusters, and ICAM-1 molecules can be found within the clusters and outside of the clusters as well.

What is the biological significance of the protein clusters described above? In most cases, there is no exact answer to this question; based on literary data, we can only presume the functional significance.

In soluble MHC:peptide multimer (dimers, trimers, and tetramers) experiments, the aggregation of MHC molecules can significantly increase the efficiency of the response in T cells. Several recent publications have reported on the location of immunological synapse molecules according to a certain order (organizing into "supramolecular" clusters) [35, 43–49]. In light of these facts, we can presume that some of the reviewed associates (e.g., the homoassociation; the HLA class II—HLA class I and the ICAM-1—HLA class I or class II heteroassociation) play a role in the process of antigen presentation and in regulating its efficiency. Their existence may promote the formation of immunological synapses; furthermore, the high local HLA concentration provided by the oligomerization of HLA molecules can significantly increase the avidity of the connection between the two cells [50].

In summary, we were able to show the existence of different protein organization structures depending on the presence/absence of the HLA-DQ6 gene, indicating its specific mode of action. In the future, it would be interesting to compare the broad levels of HLA-DQ6 antigen-mediated activation of T cells with the membrane protein distribution of B-lymphocytes. These studies will help to elucidate the surface biology of B-lymphocytes in relation to the T1D protection mechanism by the HLA-DQ6 allele.

AUTHOR CONTRIBUTIONS

József Kormos: Data curation; formal analysis; investigation; methodology; writing-original draft. **Adrienn J. Veres:** Data curation; formal analysis; investigation; methodology; writing-original draft. **László Imre:** Investigation; methodology. **László Mátyus:** Conceptualization; formal analysis; methodology; editing. **Szilvia Benkő:** Conceptualization; formal analysis; methodology, writing-review; editing. **János**

Szöllősi: Conceptualization; writing-review and editing. **Attila Jenei:** Conceptualization; project administration; resources; supervision; writing-review and editing.

ACKNOWLEDGMENT

The skillful technical assistance of A. Bagosi is gratefully acknowledged.

CONFLICT OF INTEREST STATEMENT

The authors declare no conflict of interest.

ORCID

József Kormos https://orcid.org/0009-0001-8237-2187

János Szöllősi https://orcid.org/0000-0002-7370-2543

REFERENCES

1. Pishesha N, Harmand TJ, Ploegh HL. A guide to antigen processing and presentation. Nat Rev Immunol. 2022;22:751–64.
2. Szeto C, Lobos CA, Nguyen AT, Gras S. TCR recognition of peptide–MHC-I: rule makers and breakers. Int J Mol Sci. 2021;22:68.
3. Aflalo A, Boyle LH. Polymorphisms in MHC class I molecules influence their interactions with components of the antigen processing and presentation pathway. Int J Immunogenet. 2021;48:317–25.
4. Germain RN. MHC-dependent antigen processing and peptide presentation: providing ligands for T lymphocyte activation. Cell. 1994;76:287–99.
5. Braud VM, Allan DS, McMichael AJ. Functions of nonclassical MHC and non-MHC-encoded class I molecules. Curr Opin Immunol. 1999;11:100–8.
6. Le Bouteiller P, Solier C. Is antigen presentation the primary function of HLA-G? Microbes Infect. 2001;3:323–32.
7. Germain RN, Margulies DH. The biochemistry and cell biology of antigen processing and presentation. Annu Rev Immunol. 1993;11:403–50.
8. Oldstone MB. Virus-lymphoid cell interactions. Proc Natl Acad Sci U S A. 1996;93:12756–8.
9. Shastri N, Cardinaud S, Schwab SR, Serwold T, Kunisawa J. All the peptides that fit: the beginning, the middle, and the end of the MHC class I antigen-processing pathway. Immunol Rev. 2005;207:31–41.
10. Peaper DR, Cresswell P. Regulation of MHC class I assembly and peptide binding. Annu Rev Cell Dev Biol. 2008;24:343–68.
11. Reith W, Mach B. The bare lymphocyte syndrome and the regulation of MHC expression. Annu Rev Immunol. 2001;19:331–73.
12. Reith W, Steimle V, Mach B. Molecular defects in the bare lymphocyte syndrome and regulation of MHC class II genes. Immunol Today. 1995;16:539–46.
13. Pamer E, Cresswell P. Mechanisms of MHC class I—restricted antigen processing. Annu Rev Immunol. 1998;16:323–58.
14. Yoon JW, Jun HS. Autoimmune destruction of pancreatic beta cells. Am J Ther. 2005;12:580–91.
15. Baisch JM, Weeks T, Giles R, Hoover M, Stastny P, Capra JD. Analysis of HLA-DQ genotypes and susceptibility in insulin-dependent diabetes mellitus. N Engl J Med. 1990;322:1836–41.
16. Hanafusa T, Imagawa A. Fulminant type 1 diabetes: a novel clinical entity requiring special attention by all medical practitioners. Nat Clin Pract Endocrinol Metab. 2007;3:36–45. quiz 2p following 69.
17. Bodnár A, Bacsó Z, Jenei A, Jovin TM, Edidin M, Damjanovich S, et al. Class I HLA oligomerization at the surface of B cells is controlled by exogenous beta(2)-microglobulin: implications in activation of cytotoxic T lymphocytes. Int Immunol. 2003;15:331–9.
18. Chakrabarti A, Matko J, Rahman NA, Barisas BG, Edidin M. Self-association of class I major histocompatibility complex molecules in liposome and cell surface membranes. Biochemistry. 1992;31:7182–9.
19. Ruggiero FM, Springer S. Homotypic and heterotypic in cis associations of MHC class I molecules at the cell surface. Curr Res Immunol. 2022;3:85–99.
20. Szöllösi J, Damjanovich S, Balàzs M, Nagy P, Trón L, Fulwyler MJ, et al. Physical association between MHC class I and class II molecules detected on the cell surface by flow cytometric energy transfer. J Immunol. 1989;143:208–13.
21. Szöllösi J, Damjanovich S, Goldman CK, Fulwyler MJ, Aszalos AA, Goldstein G, et al. Flow cytometric resonance energy transfer measurements support the association of a 95-kDa peptide termed T27 with the 55-kDa Tac peptide. Proc Natl Acad Sci U S A. 1987;84:7246–50.
22. Abualrous ET, Sticht J, Freund C. Major histocompatibility complex (MHC) class I and class II proteins: impact of polymorphism on antigen presentation. Curr Opin Immunol. 2021;70:95–104.
23. Damjanovich S, Vereb G, Schaper A, Jenei A, Matkó J, Starink JP, et al. Structural hierarchy in the clustering of HLA class I molecules in the plasma membrane of human lymphoblastoid cells. Proc Natl Acad Sci U S A. 1995;92:1122–6.
24. Jenei A, Varga S, Bene L, Mátyus L, Bodnár A, Bacsó Z, et al. HLA class I and II antigens are partially co-clustered in the plasma membrane of human lymphoblastoid cells. Proc Natl Acad Sci U S A. 1997;94:7269–74.
25. Sullivan KE, Stobo JD, Peterlin BM. Molecular analysis of the bare lymphocyte syndrome. J Clin Invest. 1985;76:75–9.
26. Hume CR, Shookster LA, Collins N, O'Reilly R, Lee JS. Bare lymphocyte syndrome: altered HLA class II expression in B cell lines derived from two patients. Hum Immunol. 1989;25:1–11.
27. Szentesi G, Horváth G, Bori I, Vámosi G, Szollosi J, Gáspár R, et al. Computer program for determining fluorescence resonance energy transfer efficiency from flow cytometric data on a cell-by-cell basis. Comput Methods Programs Biomed. 2004;75:201–11.
28. Bozzola JJ, Russell LD. Electron microscopy: principles and techniques for biologists. Boston, MA: Jones & Bartlett; 1992.
29. Jenei A, Kormos J, Szentesi G, Veres AJ, Varga S, Bodnár A, et al. Non-random distribution of interleukin receptors on the cell surface. ChemPhysChem. 2009;10:1577–85.
30. Ripley BD. Spatial statistics/Brian D. Ripley. New York: Wiley; 1981.
31. Ripley BD. Statistical inference for spatial processes. Cambridge: Cambridge University Press; 1988.
32. Philimonenko AA, Janácek J, Hozák P. Statistical evaluation of colocalization patterns in immunogold labeling experiments. J Struct Biol. 2000;132:201–10.
33. Schöfer C, Janácek J, Weipoltshammer K, Pourani J, Hozák P. Mapping of cellular compartments based on ultrastructural immunogold labeling. J Struct Biol. 2004;147:128–35.
34. Triantafilou K, Triantafilou M, Fernandez N. Molecular associations and microdomains in antigen-presenting cell-T-cell interactions. Crit Rev Immunol. 2000;20:359–73.
35. Cassioli C, Baldari CT. Lymphocyte polarization during immune synapse assembly: centrosomal actin joins the game. Front Immunol. 2022;13:830835.
36. Tscherning T, Claësson MH. Signal transduction via MHC class-I molecules in T cells. Scand J Immunol. 1994;39:117–21.
37. Kelly MA, Rayner ML, Mijovic CH, Barnett AH. Long-term expression of an HLA-DQ molecule in the EBV-transformed bare lymphocyte cell line, BLS-1, using a plasmid vector. Scand J Immunol. 2002;55:599–605.
38. Bene L, Balazs M, Matko J, Most J, Dierich MP, Szollosi J, et al. Lateral Organization of the Icam-1 molecule at the surface of human lymphoblasts—a possible model for its codistribution with the Il-2

receptor, class-I and class-II Hla molecules. Eur J Immunol. 1994;24:2115–23.
39. Bene L, Kanyari Z, Bodnar A, Kappelmayer J, Waldmann TA, Vamosi G, et al. Colorectal carcinoma rearranges cell surface protein topology and density in CD4(+) T cells. Biochem Biophys Res Commun. 2007;361:202–7.
40. Damjanovich S, Matko J, Matyus L, Szabo G, Szollosi J, Pieri JC, et al. Supramolecular receptor structures in the plasma membrane of lymphocytes revealed by flow cytometric energy transfer scanning force- and transmission electron-microscopic analyses. Cytometry. 1998;33:225–33.
41. Matko J, Bushkin Y, Wei T, Edidin M. Clustering of class I HLA molecules on the surfaces of activated and transformed human cells. J Immunol. 1994;152:3353–60.
42. Szollosi J, Horejsi V, Bene L, Angelisova P, Damjanovich S. Supramolecular complexes of MHC class I, MHC class II, CD20, and tetraspan molecules (CD53, CD81, and CD82) at the surface of a B cell line JY. J Immunol. 1996;157:2939–46.
43. Armony G, Heck AJR, Wu W. Extracellular crosslinking mass spectrometry reveals HLA class I - HLA class II interactions on the cell surface. Mol Immunol. 2021;136:16–25.
44. Bene L, Bagdány M, Damjanovich L. Adaptive threshold-stochastic resonance (AT-SR) in MHC clusters on the cell surface. Immunol Lett. 2020;217:65–71.
45. Bene L, Bagdány M, Damjanovich L. T-cell receptor is a threshold detector: sub- and supra-threshold stochastic resonance in TCR-MHC clusters on the cell surface. Entropy (Basel). 2022;24:24.
46. Christophersen A. Peptide–MHC class I and class II tetramers: from flow to mass cytometry. HLA. 2020;95:169–78.
47. Grakoui A, Bromley SK, Sumen C, Davis MM, Shaw AS, Allen PM, et al. The immunological synapse: a molecular machine controlling T cell activation. Science. 1999;285:221–7.
48. Monks CR, Freiberg BA, Kupfer H, Sciaky N, Kupfer A. Three-dimensional segregation of supramolecular activation clusters in T cells. Nature. 1998;395:82–6.
49. Nepom GT. MHC class II tetramers. J Immunol. 2012;188:2477–82.
50. Bromley SK, Burack WR, Johnson KG, Somersalo K, Sims TN, Sumen C, et al. The immunological synapse. Annu Rev Immunol. 2001;19:375–96.

SUPPORTING INFORMATION

Additional supporting information can be found online in the Supporting Information section at the end of this article.

How to cite this article: Kormos J, Veres AJ, Imre L, Mátyus L, Benkő S, Szöllősi J, et al. HLA DQ protein changes the cell surface distribution pattern of HLA proteins as monitored by Förster resonance energy transfer and high-resolution electron microscopy. Cytometry. 2023. https://doi.org/10.1002/cyto.a.24787